Strategies for the optimization of the oxide ion conductivities of Apatite-type germanates

A. Orera[1], T. Baikie[2], P. Panchmatia[3], T.J. White[4], J. Hanna[5], M.E. Smith[5], M.S. Islam[3], E. Kendrick[6], P.R. Slater[1]

[1]School of Chemistry, University of Birmingham, Birmingham, U.K.
[2]School of Materials Science and Engineering, Nanyang Technological Institute, Singapore
[3]Department of Chemistry, University of Bath, Bath, U.K.
[4] Electron Microscopy Unit, Research School of Biological Sciences, Australian National University, Canberra, Australia
[5] Department of Physics, University of Warwick, Coventry, U.K.
[6]Chemical Sciences, University of Surrey, Guildford, Surrey, GU2 7XH, UK

Abstract

Recently apatite-type germanates, $La_{9.33+x}Ge_6O_{26+3x/2}$ have been attracting considerable interest due to their high oxide ion conductivities. Research has shown that the key defects are oxide ion interstitials which lead to the conversion of some of the GeO_4 units to GeO_5. Consequently there has been a large interest in the preparation of high oxygen excess samples to achieve high defect concentration. This strategy, however, leads to a reduction in symmetry from hexagonal to triclinic for x>0.4, and consequently to reduced oxide ion conductivity at low temperatures. In this paper, we present doping strategies to stabilize the hexagonal lattice, while maintaining high oxygen content. In particular, partial substitution of La by smaller rare earths (Y, Yb) is shown to be successful in preparing x=0.67 samples with hexagonal symmetry and hence high conductivities. In addition, doping on the Ge site with Ti, Nb, or W, has been shown to be similarly successful in this respect, leading to very high oxygen contents for W doping, e.g. $La_{10}Ge_{5.5}W_{0.5}O_{27.5}$. In the case of Ti doping, however, there was some evidence for trapping of the interstitial oxide ions around the Ti, similar to observed for Ti doping in related silicate apatites. Preliminary results on the effect of similar doping strategies on Pr, Nd germanates, $(Pr.Nd)_{9.33+x}Ge_6O_{26+3x/2}$, are also discussed.

Introduction

With the growing concerns regarding increasing greenhouse gas emissions and their effect on climate change, there has been substantial interest in the demonstration and utilisation of solid oxide fuel cell systems. Traditionally the electrolyte utilised in such systems has been fluorite-type, e.g. yttria stabilised zirconia, rare earth doped ceria, although perovskite systems, e.g. $LaGaO_3$, have also attracted substantial interest [1]. In all these systems, the ionic conduction is mediated by oxide ion vacancy defects, introduced by aliovalent doping. More recently there has been growing interest in materials, whose conduction process is mediated by oxide ion interstitials [2], an important example being apatite-type silicates/germanates, $Ln_{9.33+x}(Si/GeO_4)_6O_{2+3x/2}$ (Ln=rare earth) (figure 1). The vast majority of the work has so far focused on the silicate systems, although the germanates show some benefits in terms of higher conductivities at elevated temperatures, lower synthesis/sintering temperatures, and higher oxygen interstitial contents achievable [3-35]. In terms of the germanates it has been shown that $Ln_{9.33+x}(GeO_4)_6O_{2+3x/2}$ samples with x up to 0.67 can be prepared, whereas for the silicates, the limit is close to x=0.33. However, one complexity of these high oxygen excess germanates is a change in symmetry from hexagonal to triclinic as x increases. Thus it has been shown that single phase samples of $La_{9.33+x}(GeO_4)_6O_{2+3x/2}$ with hexagonal symmetry can be prepared for $x \leq 0.42$, while samples with $x>0.42$ exhibit a triclinic cell [4,6,11,14]. A consequence of the lower symmetry cell is a reduction in the conductivity at low temperatures, attributed to enhanced defect trapping, which is a problem in terms of applications [4]. The origin of the triclinic distortion can be explained from a consideration of the structures of these systems, which may be classed as "microporous" framework ($La_{3.33+x}(GeO_4)_6$) composed of face sharing

LaO_6 trigonal meta-prismatic columns, that are corner connected to the GeO_4 tetrahedra [13]. The remaining La_6O_2 units occupy the "cavities" within this framework, while the excess interstitial oxide ions (3x/2) are located within the framework. The triclinic distortion can then be explained by a mismatch between the size of the framework and the La_6O_2 units in the cavities, leading to underbonding at these latter La sites, which is alleviated by the tilting of the tetrahedra in the triclinic cell [13]. The excess oxygen, being located within the framework, enhances this mismatch and hence samples with high x give triclinic cells. Confirmation of this latter aspect comes from nitridation studies of the $La_{10}Ge_6O_{27}$, which showed that the introduction of N lowers the total anion content ($2N^{3-}$ replace $3O^{2-}$), removing the interstitial anions, and hence increasing the symmetry from triclinic to hexagonal [27]. The results outlined above highlight the need to consider two competing factors when designing apatite germanates with high conductivities: oxide ion interstitials are required for high conductivity, and hence there is an incentive to increase the oxygen content, but this can lead to a triclinic cell and hence defect trapping. Consequently we have been investigating doping strategies towards achieving high oxygen contents, while maintaining hexagonal symmetry. Initial work focused on doping on the La site, and it was shown that by doping with the smaller rare earth, Y, it is possible to prepare such high oxygen contents samples with hexagonal symmetry, e.g. $La_8Y_2(GeO_4)_6O_3$ [18]. In this paper, we present further work on similar La site dopants. In addition, we show that it is also possible to prepare high oxygen excess hexagonal samples through doping on the Ge site with Ti, Nb, W. Preliminary results on the effect of such doping strategies on related $(Pr/Nd)_{9.33+x}(GeO_4)_6O_{2+3x/2}$ systems are also presented.

Experimental

Samples were prepared by solid state reaction from dried La_2O_3, Pr_6O_{11}, Nd_2O_3, Y_2O_3, Yb_2O_3, Gd_2O_3, Sm_2O_3, GeO_2, Nb_2O_5, WO_3, TiO_2 starting materials, using two consecutive 10h firing stages at 1100°C with intermediate regrind and a final heating at 1300-1400°C for 2 hours. Phase purity was confirmed by X-ray powder diffraction (Bruker D8 diffractometer or Panalytical X'Pert Pro diffractometer, Cu $K\alpha_1$ radiation).

Conductivity measurements were made on the pellets using AC impedance spectroscopy (Hewlett Packard 4182A impedance analyser) in the range from 0.1 to 10^3 kHz. The collected impedance data were analysed using equivalent circuits to separate both bulk and grain boundary contributions to the resistance, and the data presented represents bulk conductivities.

Results and Discussion

Doping on the La site with smaller rare earths: $La_{10-x}(RE)_x(GeO_4)_6O_3$ (RE=Y, Yb, Gd, Sm, Nd)

Our prior work showed that doping with Y on the La site, $La_{10-x}Y_x(GeO_4)_6O_3$, in the range $1 \leq x \leq 3$, was successful in stabilizing the hexagonal cell, although higher levels of Y resulted in the observation of a triclinic cell, as for the parent phase [18]. Cell parameter calculations for the hexagonal phases showed that the Y doping led to a significant reduction in the c axis length, while there was only a small decrease along a/b [18]. Conductivity measurements showed that the hexagonal Y doped samples had high conductivities over the full range of temperatures examined. In comparison, the triclinic

$La_6Y_4(GeO_4)_6O_3$ had a low conductivity at low temperatures, attributed to defect trapping in the triclinic cell. The conductivity then increased at high temperatures, due to a change in symmetry to hexagonal as observed for the undoped $La_{10}(GeO_4)_6O_3$ parent material. Similar stabilization of the hexagonal lattice was also observed in this study on doping with Yb, which is slightly smaller than Y. However, larger rare earths such as Gd, Sm and Nd were not successful in this respect, and in these cases a triclinic cell was observed as for the undoped parent phase. Thus the size of the rare earth dopant is key to the stabilization of the hexagonal lattice, with ions with radii (9 coordination) < 1.1 Å required (Figure 1). The effect of this stabilization of the hexagonal phase on the ionic conductivity is shown in figure 2, which compares conductivity data for $La_8RE_2(GeO_4)_6O_3$ (RE=Gd, Yb, Y) samples. The samples with RE=Y, Yb show high conductivities over the whole temperature range studied, consistent with hexagonal symmetry, while for the Gd-substituted sample, the conductivity at low temperatures is much lower, as a result of defect trapping in the low symmetry triclinic cell. At higher temperatures, where this sample becomes hexagonal, the conductivity is now comparable to the Y, Yb doped samples.

The stabilization of the hexagonal lattice has been attributed to the smaller rare earth preferentially substituting into the framework sites (supported by neutron diffraction studies of Y doped systems, and modeling studies which showed a preference for smaller rare earths to dope into the framework La sites), thus reducing the size of this framework and hence reducing the mismatch between the La_6O_2 units in the channels.

Ti substitution: $La_{10}(GeO_4)_{6-x}(TiO_4)_xO_3$

The results showed that it was possible to introduce a large level of Ti into the structure, with single phase samples observed for $x \leq 2.0$, which corresponds to a similar maximum level of Ti substitution to that of the related apatite silicates [31]. The X-ray diffraction data showed that as the Ti content was increased the cell symmetry changed from triclinic ($x < 1$) to hexagonal ($x > 1$) (figure 3). As the triclinic distortion decreases on Ti substitution for $0<x<1$, there was an increase in the low temperature conductivity. However, for $x> 1$, where all samples are now hexagonal, a general decrease in the magnitude of the conductivity was observed (Figure 4a). This decrease in conductivity for high levels of Ti substitution is most likely related to trapping of the interstitial oxide ions around the Ti dopant, and such an effect was also observed in the corresponding silicate series $La_{10}(SiO_4)_{6-x}(TiO_4)_xO_3$ [31], although in these latter systems the decrease in conductivity was far more pronounced. The effect of this proposed oxide ion interstitial defect trapping would be to decrease the number of charge carriers that are available for conduction, and evidence in support of this can also be clearly seen in the comparison of the conductivity values at 830°C (Figure 4b). At this temperature, all the compositions examined have hexagonal symmetry and the same nominal interstitial oxygen content, and the data clearly shows a decrease in conductivity with increasing Ti content. Thus there are two competing factors on the conductivity in Ti doped samples;

1. the presence of Ti stabilizing the hexagonal lattice and so leading to enhanced low temperature conductivities with increasing Ti content for $0 \leq x \leq 1$.
2. Trapping of the interstitial oxide ion defects around the Ti dopant (e.g. as either TiO_5 units) leads to a reduction in the number of mobile defects and hence a decrease in the high temperature conductivity across the whole range $0 \leq x \leq 2$.

The effect of these two features can be seen in figure 5, comparing Arrhenius plots for x=0.25, 1.0, and 2.0 samples. In these plots it can be seen that the x=1 sample has the highest low temperature conductivity due to the stabilization of the hexagonal lattice, while x=2 has the lowest conductivity due to the increase in Ti content outweighing the beneficial effect from hexagonal symmetry leading to maximum trapping of the oxide ion interstitial defects. The x=0.25 sample shows low conductivity at low temperature, due to the lower symmetry triclinic cell, while at high temperature, where the sample is hexagonal, the conductivity is highest of the three, due to the lowest Ti content.

With regard to the stabilization of the hexagonal lattice, it is interesting that Ti is successful in this respect, since the opposite might have been expected. Ti is slightly larger than Ge (ionic radii 0.605 and 0.53 Å respectively), and hence will increase the size of the framework, which might therefore be expected to increase the mismatch with the La_6O_2 units in the channels, and hence increase the triclinic distortion, as observed on doping with large lower valent ions such as Ga, Co [4, 18]. Clearly, this is not the case, and detailed structural studies are therefore required to account for this discrepancy.

Nb substitution: $La_{10-y}(GeO_4)_{6-x}(NbO_4)_xO_{3-3y/2+x/2}$

As for Ti doping, Nb substitution according to the formula $La_{10}(GeO_4)_{6-x}(NbO_4)_xO_{3+x/2}$, was shown to lead to a stabilization of the hexagonal phase, although in this case it was only possible to introduce a limited amount of Nb, $x \leq 0.5$. In the case of the composition with the highest substitution level, x=0.5, a small amount of La_3NbO_7 impurity was observed, which could be eliminated by reducing the La content slightly, the composition $La_{9.83}(GeO_4)_{5.5}(NbO_4)_{0.5}O_3$ being single phase. The Nb doping was shown to enhance the

conductivity at low temperatures as a result of such doped samples having a higher symmetry hexagonal cell (Figure 6). As for the Ti doping, the stabilization of the hexagonal cell was somewhat unexpected given the larger size of Nb versus Ge (0.64 vs 0.53 Å). Neutron diffraction data have been recently collected for the sample of nominal composition, $La_{9.83}(GeO_4)_{5.5}(NbO_4)_{0.5}O_3$ with a view to understanding this feature.

W substitution: $La_{10}(GeO_4)_{6-x}(WO_4)_xO_{3+x}$

The results from the W doping studies indicated that it was possible to introduce similar levels of W as for Nb, $x \leq 0.5$, although in this case it was not necessary to lower the La content to achieve single phase samples. As for Ti and Nb, doping with W ($x=0.5$) was shown to stabilize the hexagonal lattice leading to enhanced conductivity at low temperature in comparison to the undoped phase. As a result of the higher charge on W versus Ge, this also leads to a significant enhancement of the oxygen content, and hence interstitial level. Despite this significant increase in oxygen content, there is no significant change in the conductivity compared with high oxygen content hexagonal samples, doped on the La site, $La_8Y_2(GeO_4)_6O_3$ (Figure 7). This would suggest that either there is a limit to the increase in conductivity on increasing oxygen content, such that there is an optimum oxygen interstitial content, or there could be partial trapping of the interstitial oxide ion defects by W, as was proposed in the case of Ti doping, which counterbalances the effect of the increase in oxygen content. Further studies, including dopant-defect association atomistic simulations are planned to investigate this feature in more detail.

Preparation of $(Nd/Pr)_{9.33+x}(GeO_4)_6O_{2+3x/2}$ systems

Despite the large interest in these $La_{9.33+x}(GeO_4)_6O_{2+3x/2}$ apatite germanates, there have been no reports of the effect on the conductivity of completely replacing La by smaller rare earths such as Pr, Nd, and so preliminary studies on such systems were performed. In contrast to the observation of hexagonal cells for $La_{9.33+x}(GeO_4)_6O_{2+3x/2}$ in the range $0 \leq x \leq 0.4$ [6], all $(Nd/Pr)_{9.33+x}(GeO_4)_6O_{2+3x/2}$ samples irrespective of oxygen content were found to display triclinic symmetry. Conductivity data showed low values at low temperatures consistent with the triclinic symmetry (figure 8). Moreover, the conductivities for the Nd containing systems were significantly lower than for the Pr analogue, suggesting that as for the silicate apatites, there is a reduction in conductivity with decreasing rare earth size [4]. Attempts at stabilizing the hexagonal lattice for these series using similar strategies as for the high oxygen content $La_{9.33+x}(GeO_4)_6O_{2+3x/2}$ series (e.g. Y doping for Pr, Nd; Ti, W, Nb doping for Ge) were all unsuccessful. The hexagonal lattice could be obtained by Sr substitution, i.e. $(Nd/Pr)_8Sr_2(GeO_4)_6O_2$ but the lack of interstitial oxide ion defects in such phases meant that the conductivities were low.

Conclusions

Apatite-type lanthanum germanates, $La_{9.33+x}(GeO_4)_6O_{2+3x/2}$, are interstitial oxide ion conductors, which show a wide solid solution and hence oxide ion interstitial range. The presence of large levels of interstitial oxide ions ($x>0.4$) leads however to a reduction in symmetry to triclinic and hence reduced low temperature conductivity, attributed to defect trapping. The results reported here show that through doping with Y, Yb on the La

site, or Ti, Nb, W on the Ge site, high oxygen content samples with hexagonal symmetry can be prepared leading to an enhancement in the low temperature conductivity. In the case of Ti doping, however, there was evidence to suggest some defect trapping around the dopant, similar to reported for related Ti doped silicate systems. Attempts to prepare high oxygen content Pr, Nd analogues, $(Nd/Pr)_{9.33+x}(GeO_4)_6O_{2+3x/2}$, with hexagonal symmetry were unsuccessful, hence suggesting that work aimed at improving the oxide ion conductivities of apatite germanates be limited to the La based system.

Acknowledgements

We would like to thank EPSRC for funding (grant EP/F015178/1). The X-ray diffractometer used in this research was obtained through the Science City Advanced Materials project: Creating and Characterising Next generation Advanced Materials project, with support from Advantage West Midlands (AWM) and part funded by the European Regional Development Fund (ERDF)

References

[1] J.B. Goodenough, *Annu. Rev. Mater. Res.* **2003**, *33*, 91

[2] A. Orera, P.R. Slater, *Chem. Mater*. (in press).

[3] S. Nakayama, H. Aono, Y. Sadaoka, *Chem. Lett*. **1995**, 431.

[4] E. Kendrick, M.S. Islam, P.R. Slater; *J. Mater. Chem*. **2007**, *17*, 3104.

[5] J.E.H. Sansom, D. Richings, P.R. Slater, *Solid State Ionics* **2001**, *139*, 205.

[6] L. Leon-Reina, M.C. Martin-Sedeno, E.R. Losilla, A. Cabeza, M. Martinez-Lara, S. Bruque, F.M.B. Marques, D.V. Sheptyakov, M.A.G. Aranda; *Chem. Mater*. **2003**, *15*, 2099.

[7] L. Leon-Reina, E.R. Losilla, M. Martinez-Lara, S. Bruque, M.A.G. Aranda; *J. Mater. Chem*. **2004**, *14*, 1142.

[8] J.R. Tolchard, M.S. Islam, P.R. Slater; *J. Mater. Chem*. **2003**, *13*, 1956.

[9] J.E.H. Sansom, J.R. Tolchard, D. Apperley, M.S. Islam, P.R. Slater; *J. Mater. Chem*. **2006**, *16*, 1410.

[10] L. Leon-Reina, J.M. Porras-Vasquez, E.R. Losilla, M.A.G. Aranda; *J. Solid State Chem*. **2007**, *180*, 1250.

[11] S. S. Pramana, W.T. Klooster and T. J. White; *Acta Crystallogr. B* **2007**, *63*, 597.

[12] E. Kendrick, M.S.Islam, P.R. Slater; *Chem. Commun* **2008**, 715.

[13] T. Baikie, P.H.J. Mercier, M.M. Elcombe, J.Y. Kim, Y. Le Page, L.D. Mitchell, T.J. White, P.S. Whitfield, *Acta Crystallogr. B* **2007**, *63*, 251

[14] S.S. Pramana, W.T. Klooster, T.J. White; *J. Solid State Chem*. **2008**, *181*, 1717.

[15] A. Orera, E. Kendrick, D. C. Apperley, V.M. Orera, P.R. Slater; *Dalton Trans*. **2008** 5296.

[16] J.E.H. Sansom, P.R. Slater; *Solid State Ionics* **2004**, *167*, 23.

[17] H. Yoshioka; *J. Amer. Ceram. Soc*. **2007**, *90*, 3099.

[18] E. Kendrick, P.R. Slater; *Mater. Res. Bull*. **2008**, *43*, 2509.

[19] E. Kendrick, P.R. Slater; *Solid State Ionics* **2008**, *179*, 981.

[20] P.J. Panteix, I. Julien, P. Abelard, D. Bernache-Assolant; *Ceram. Int*. **2008**, *34*, 1579.

[21] T. Iwata, K. Fukuda, E. Bechade, O. Masson, I. Julien, E. Champion, P. Thomas; *Solid State Ionics* **2008**, *178*, 1523.

[22] R. Ali, M. Yashima, Y. Matsushita, H. Yoshioka, K. Okoyama, F. Izumi; *Chem. Mater*. **2008**, *20,* 5203.

[23] E. Kendrick, D. Headspith, A. Orera, D.C. Apperley, R.I. Smith, M.G. Francesconi, P.R. Slater; *J. Mater. Chem*. **2009**, *19*, 749.

[24] E. Rodriguez-Reyna, A.F. Fuentes, M. Maczka, J. Lanuza, K. Boulahya, U. Amador; *Solid State Sci.* **2006**, *8*, 168-177.

[25] L. Leon-Reina, E.R. Losilla, M. Martinez-Lara, S. Bruque, A. Llobet, D.V. Sheptyakov, M.A.G. Aranda; *J. Mater. Chem*. **2005**, *15*, 2489.

[26] P.R. Slater, J.E.H. Sansom, J.R. Tolchard; *Chem. Record* **2004**, *4(6)*, 373

[27] A. Orera, D. Headspith, D.C. Apperley, M.G. Francesconi, P.R. Slater; *J. Solid State Chem*. **2009**, *182*, 3294.

[28] E. Kendrick, K.S. Knight, P.R. Slater; *Mater. Res. Bull*. **2009**, *44*, 1806.

[29] J.M. Porras-Vazquez, E.R. Losilla, L. Leon-Reina, D. Marrero-Lopez, M.A.G. Aranda; *J. Am. Ceram. Soc*. **2009**, *92*, 1062.

[30] C. Bonhomme, S. Beaudet-Savignat, T. Chartier, P-M. Geffroy, A-L. Sauvet ; *J. Euro. Ceram. Soc*. **2009**, *29*, 1781.

[31] A. Al-Yasari, A. Jones, D.C. Apperley, D. Driscoll, M.S. Islam, P.R. Slater; *J. Mater. Chem*. **2009**, *19*, 5003.

[32] E. Bechade, O. Masson, T. Iwata, I. Julien, K. Fukuda, P. Thomas, E. Champion; *Chem. Mater*. **2009**, *21*, 2508.

[33] E. Kendrick, A. Orera, P.R. Slater ; *J. Mater. Chem*. **2009**, *19*, 7955.

[34] S. S. Pramana, T. J. White, M. K. Schreyer, C. Ferraris, P. R. Slater, A. Orera, T. J. Bastow, S. Mangold, S. Doyle, T. Liu, A. Fajar**,** M. Srinivasan, T. Baikie; *Dalton Trans*. **2009**, *39*, 8280.

[35] S. Guillot, S. Beaudet-Savignat, S. Lambert, R-N. Vannier, P. Roussel, F. Porcher; *J. Solid State Chem*. **2009**, *182*, 3358.

Figure 1. Effect of rare earth dopant size on the stabilization of the hexagonal phase for compositions $La_8RE_2(GeO_4)_6O_3$

Figure 2. Arrhenius plot of the bulk conductivity data for $La_8RE_2(GeO_4)_6O_3$ (RE = Y, Yb Gd), showing enhanced low temperature conductivities for RE=Y, Yb, due to stabilization of the hexagonal lattice.

Figure 3. X-ray diffraction patterns of $La_{10}(GeO_4)_{6-x}(TiO_4)_xO_3$ (x = 0, 0.5, 1.5).

Figure 4. Variation in bulk conductivities of $La_{10}(GeO_4)_{6-x}(TiO_4)_xO_3$ at (a) 430°C and (b) 830°C.

Figure 5. Comparison of the bulk conductivities of $La_{10}(GeO_4)_{6-x}(TiO_4)_xO_3$, x = 0.25, 1, 2.

Figure 6. Arrhenius plot of the bulk conductivity data for $La_{9.83}(GeO_4)_{5.5}(NbO_4)_{0.5}O_3$

Figure 7. Comparison of the bulk conductivities of $La_8Y_2Ge_6O_{27}$ and $La_{10}Ge_{5.5}W_{0.5}O_{27.5}$

Figure 8. Comparison of the bulk conductivities for $Pr_{9.5}Ge_6O_{26.25}$ and $Nd_{9.5}Ge_6O_{26.25}$

Figure 1

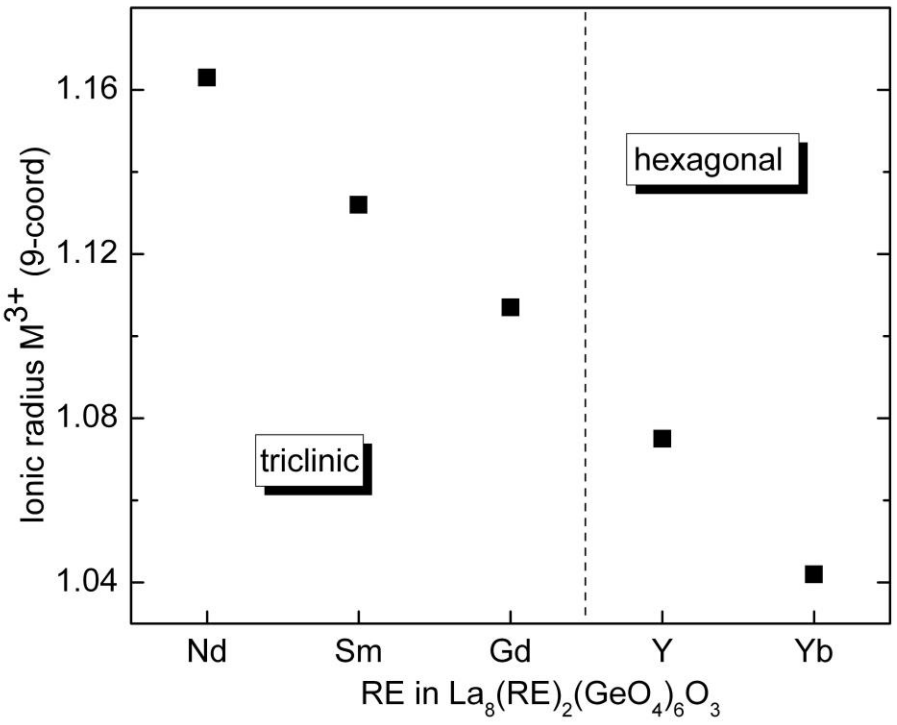
1.16
1.12
1.08
1.04
Ionic radius M^{3+} (9-coord)
hexagonal
triclinic
Nd
Sm
Gd
Y
Yb
RE in $La_8(RE)_2(GeO_4)_6O_3$

Figure 2

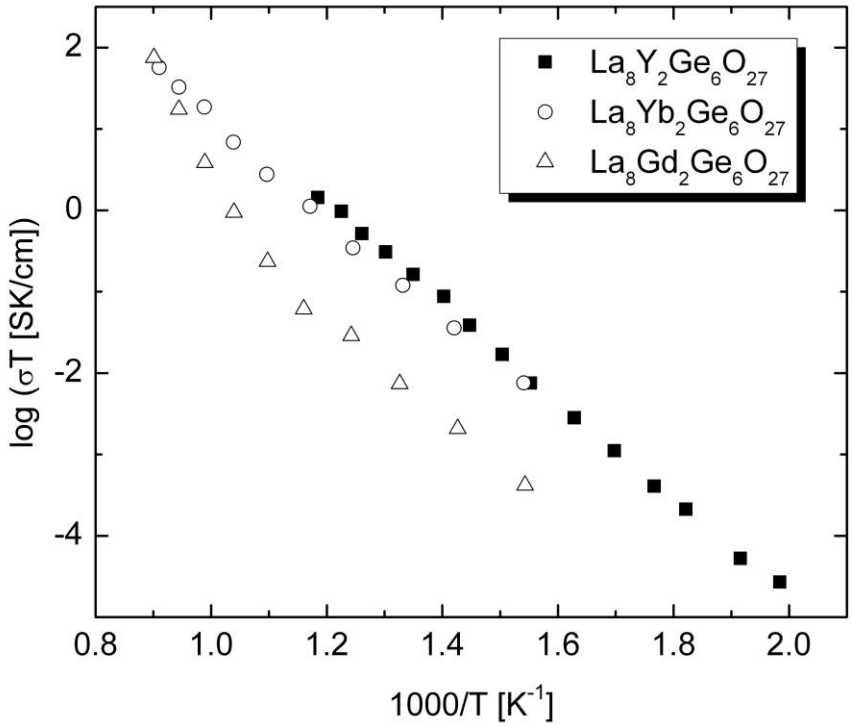
2
0
-2
-4
0.8
1.0
1.2
1.4
1.6
1.8
2.0
log (σT [SK/cm])
1000/T [K-1]
La8Y2Ge6O27
La8Yb2Ge6O27
La8Gd2Ge6O27

Figure 3

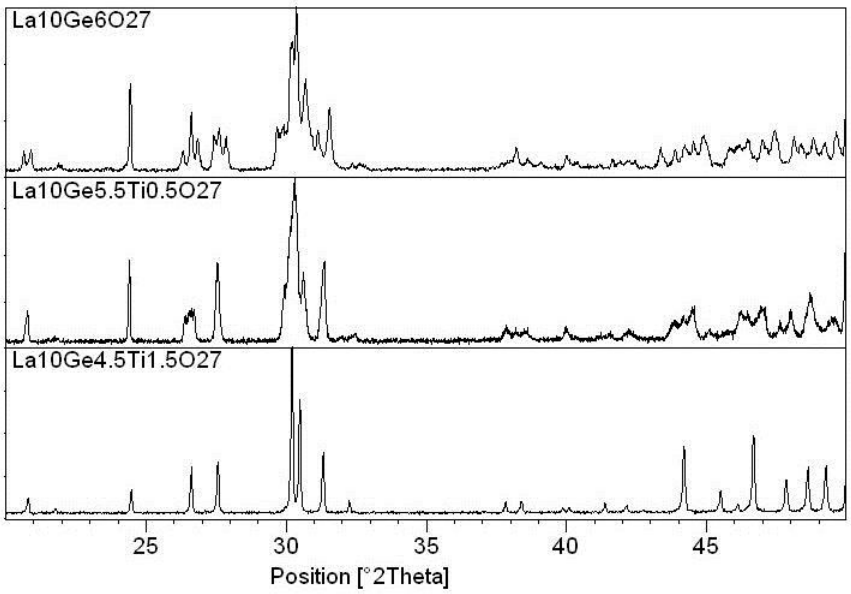
La10Ge6O27
La10Ge5.5Ti0.5O27
La10Ge4.5Ti1.5O27
25
30
35
40
45
Position [°2Theta]

Figure 4
(a)

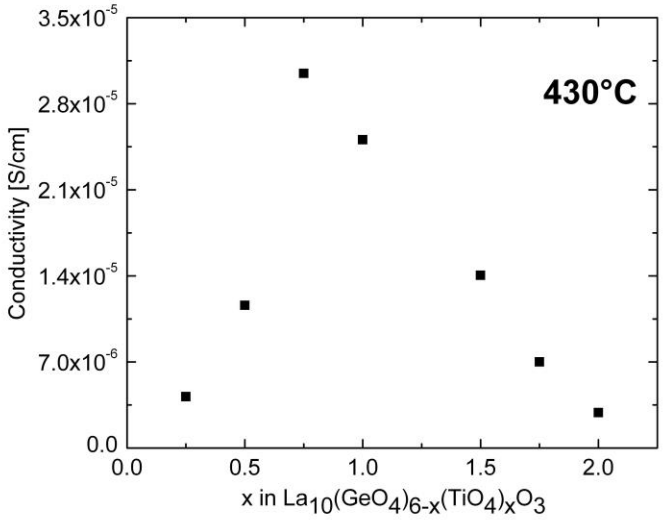
3.5x10-5
2.8x10-5
2.1x10-5
1.4x10-5
7.0x10-6
0.0
Conductivity [S/cm]
430°C
0.0
0.5
1.0
1.5
2.0
x in La10(GeO4)6-x(TiO4)xO3

(b)

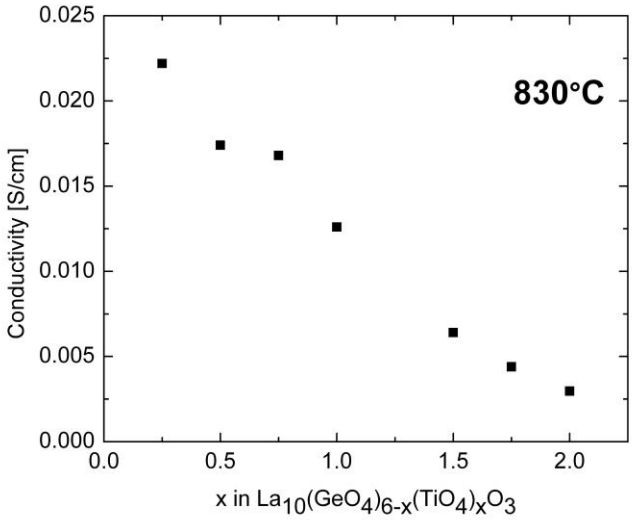
0.025
0.020
0.015
0.010
0.005
0.000
Conductivity [S/cm]
830°C
0.0
0.5
1.0
1.5
2.0
x in La10(GeO4)6-x(TiO4)xO3

Figure 5

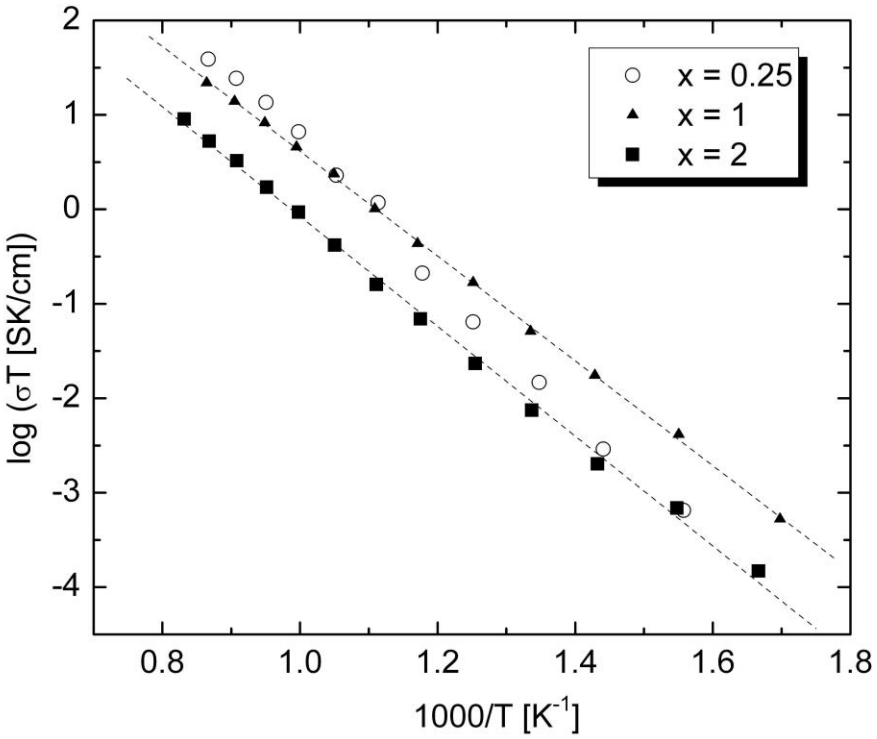

Figure 6

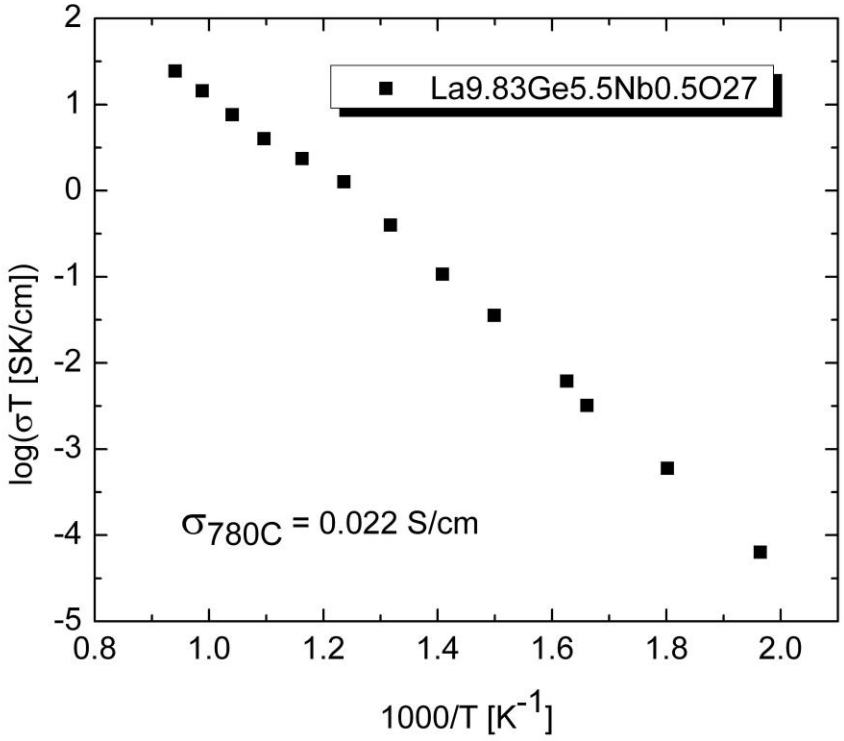
La9.83Ge5.5Nb0.5O27
σ780C = 0.022 S/cm
log(σT [SK/cm])
1000/T [K-1]
2
1
0
-1
-2
-3
-4
-5
0.8
1.0
1.2
1.4
1.6
1.8
2.0

Figure 7

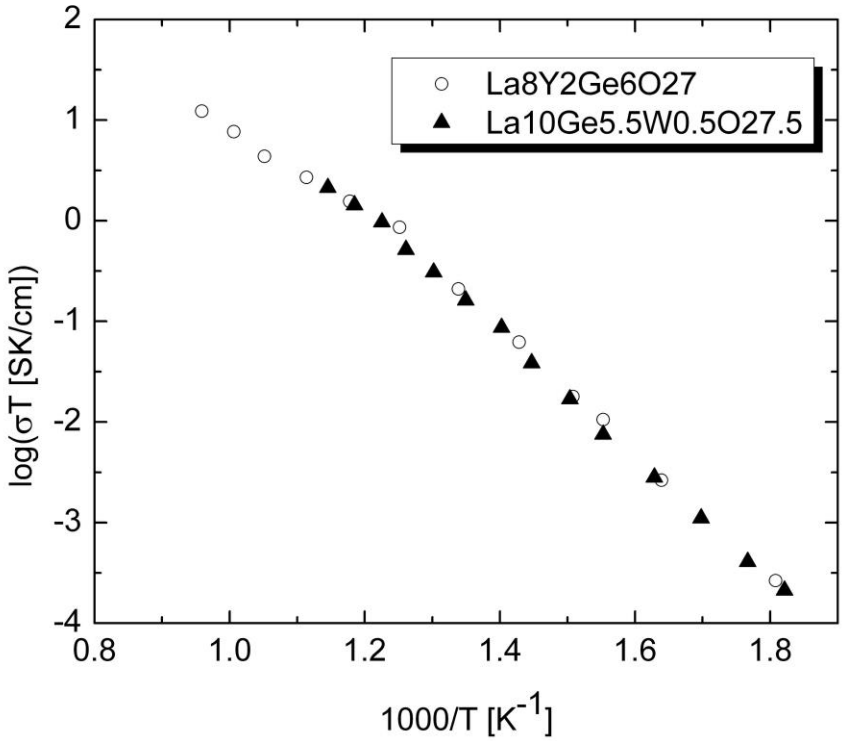
La8Y2Ge6O27
La10Ge5.5W0.5O27.5
log(σT [SK/cm])
1000/T [K-1]
2
1
0
-1
-2
-3
-4
0.8
1.0
1.2
1.4
1.6
1.8

Figure 8

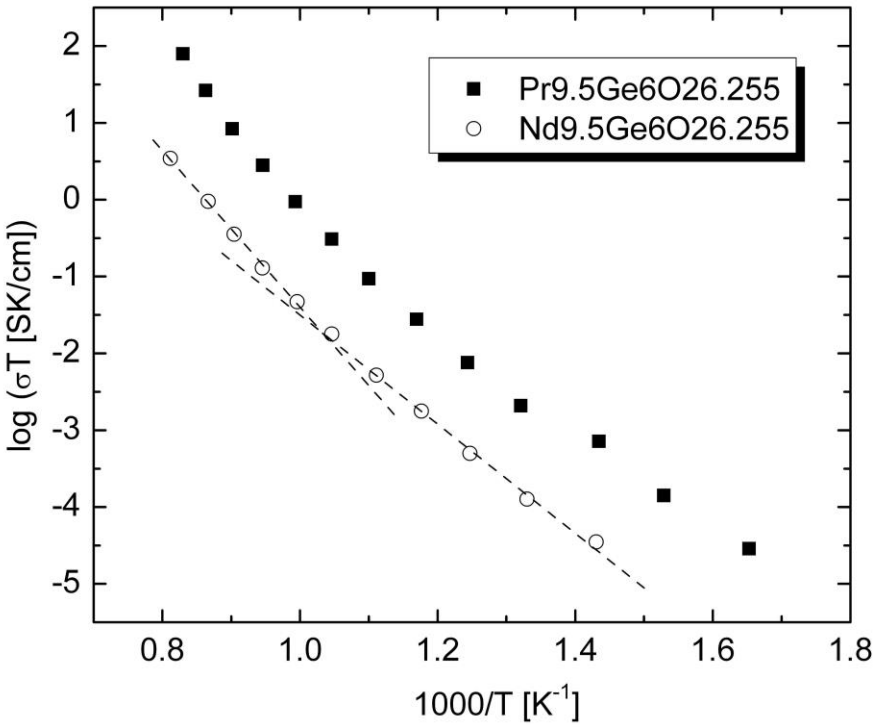
Pr9.5Ge6O26.255
Nd9.5Ge6O26.255
log (σT [SK/cm])
1000/T [K-1]
2
1
0
-1
-2
-3
-4
-5
0.8
1.0
1.2
1.4
1.6
1.8